Flexoelectricity in atomic monolayers from first principles

Journal:	*Nanoscale*
Manuscript ID	NR-COM-11-2020-007803.R1
Article Type:	Communication
Date Submitted by the Author:	27-Nov-2020
Complete List of Authors:	Kumar, Shashikant; Georgia Institute of Technology Codony, David; Universitat Politecnica de Catalunya Arias, Irene; Universitat Politecnica de Catalunya Suryanarayana, Phanish; Georgia Institute of Technology

SCHOLARONE™
Manuscripts

Journal Name

Flexoelectricity in atomic monolayers from first principles[†]

Shashikant Kumar,[a] David Codony,[b] Irene Arias,[b,c] and Phanish Suryanarayana[*a]

We study the flexoelectric effect in fifty-four select atomic monolayers using ab initio Density Functional Theory (DFT). Specifically, considering representative materials from each of Group III monochalcogenides, transition metal dichalcogenides (TMDs), Groups IV, III-V, V monolayers, Group IV dichalcogenides, Group IV monochalcogenides, transition metal trichalcogenides (TMTs), and Group V chalcogenides, we perform symmetry-adapted DFT simulations to calculate transversal flexoelectric coefficients along the principal directions at practically relevant bending curvatures. We find that the materials demonstrate linear behavior and have similar coefficients along both principal directions, with values for TMTs being up to a factor of five larger than graphene. In addition, we find electronic origins for the flexoelectric effect, which increases with monolayer thickness, elastic modulus along bending direction, and sum of polarizability of constituent atoms.

Flexoelectricity[1–8] is an electromechanical property common to semiconductors/insulators that represents a two-way coupling between strain gradients and polarization. Unlike piezoelectricity, it is not restricted to materials that are non-centrosymmetric, i.e., lattice structures that do not possess inversion symmetry, and in contrast to electrostriction, it permits reversal of the strain by reversal of the electric field and allows for sensing in addition to actuation. Though the flexoelectric effect is generally negligible for bulk systems, it becomes significant in nanostructures/nanomaterials due to the possibility of extremely large strain gradients, especially along the directions in which the system has dimensions at the nanoscale.

The flexoelectric effect in two-dimensional materials has a number of applications — analogous to those found for other such electromechanical couplings[9–13] — including sensors, actuators, and energy harvestors in nanoelectromechanical systems. Even in applications where the flexoelectric effect is not being exploited, e.g., flexible electronics[14–17], nanoelectromechanical devices[18–21], and nanocomposites[22,23], the presence of strain gradients such as those encountered during bending — a common mode of deformation in two-dimensional materials, given their relatively low bending moduli values[24] — makes flexoelectricity an important design consideration[25,26]. This is evidenced by recent work where flexoelectricity has been shown to produce incorrect measurements of piezoelectric coefficients at the nanoscale[27].

Atomic monolayers, which are two-dimensional materials consisting of a single layer of material, have been the subject of intensive research over the past two decades[31–33], with dozens of monolayers having now been synthesized[34–39] and the potential for thousands more as predicted by ab initio calculations[40,41]. The widespread interest in these systems is a consequence of their novel and exciting properties[34,35,37,38,42–45], which makes them ideal candidates for the aforementioned applications. However, the transversal flexoelectric coefficients for atomic monolayers — the relevant component of the flexoelectric tensor in the context of bending deformations — are far from being established.

Experimental data for the transversal flexoelectric coef-

[a] College of Engineering, Georgia Institute of Technology, Atlanta, GA 30332, USA. E-mail: phanish.suryanaryana@ce.gatech.edu

[b] Laboratori de Càlcul Numèric, Universitat Politècnica de Catalunya, Barcelona, E-08034, Spain

[c] Centre Internacional de Metodes Númerics en Enginyeria (CIMNE), 08034 Barcelona, Spain
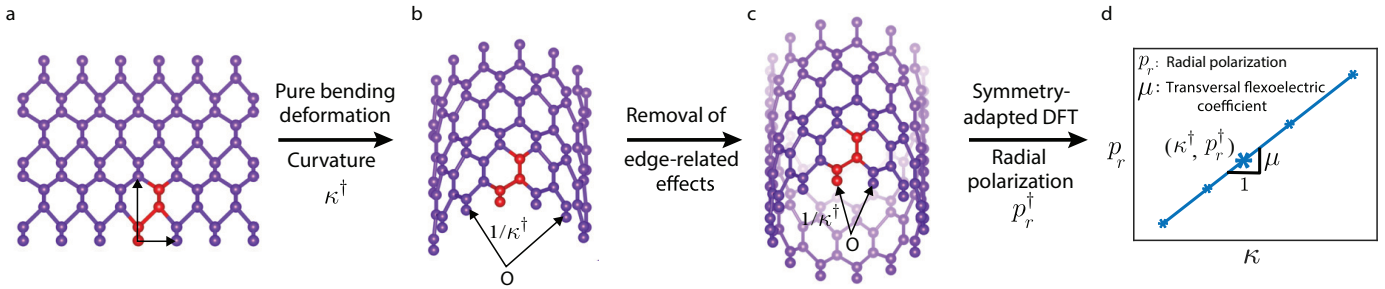
Fig. 1 Schematic illustrating the calculation of transversal flexoelectric coefficient for atomic monolayers using symmetry-adapted DFT simulations [28–30]. The atoms in the unit cell are colored red.

ficients of atomic monolayers is highly sparse, likely due to the challenges associated with isolating the flexoelectric and piezoelectric contributions [46]. Recently, the coefficients for some TMDs (MX$_2$: M=Mo,W; X=S,Se) have been measured [46,47], however there is significant uncertainty in the results, due to large error bars and the use of substrates. On the theoretical side, studies based on ab initio Kohn-Sham DFT [48,49] have been used to calculate the flexoelectric coefficients of graphene [4,50–52] and some TMDs (MX$_2$: M=Mo,W; X=S,Se,Te) [52]. However, as shown in recent work [28], the accuracy of these results is limited by the use of an ill defined flexoelectric coefficient [51,52], artificial partitioning of the electron density [50,53], and/or geometries with non-uniform strain gradients [52]. Note that a theoretically more involved alternative is provided by density-functional perturbation theory (DFPT) [54,55] — found to have significant success in the study of bulk like three-dimensional systems [56–61] — which has very recently been extended to the study of two-dimensional systems [62]. Other theoretical efforts include the use of force fields [63,64], which differ by more than an order of magnitude from experimental/DFT results, suggesting that they are unsuitable in the current context.

In this work, using a recently developed formulation for the accurate computation of the transversal flexoelectric coefficient at finite deformations [28], we perform a comprehensive first principles DFT study of the flexoelectric effect in atomic monolayers. Specifically, we compute the coefficients for fifty-four select atomic monolayers along their principal directions at practically relevant bending curvatures [65–68]. We also provide fundamental insights into the flexoelectric effect for these materials and the variation in the coefficient values between them.

The transversal flexoelectric coefficient at finite bending deformations is defined as: [28]

$$\mu = \frac{\partial p_r}{\partial \kappa}, \tag{1}$$

where p_r is the *radial polarization* and κ is the curvature. In the context of electronic structure calculations like DFT, the radial polarization can be expressed as: [28]

$$p_r = \frac{1}{A} \int_\Omega (r - R_{\text{eff}}) \rho(\mathbf{x}) \, d\mathbf{x}, \tag{2}$$

where A is the cross-sectional area of the deformed sheet within the domain Ω, r is the radial coordinate of the spatial point $\mathbf{x}$, R_{eff} is the *radial centroid* of the ions, and $\rho(\mathbf{x})$ is the electron density. Note that the *radial dipole moment* has been normalized using the area rather than the volume, as is common practice, given the significant disagreement associated with the thickness of atomic monolayers [69].

We calculate the flexoelectric coefficient by using a numerical approximation for the derivative in Eq. 1, the alternative being the more involved DFPT-based approaches, for which a symmetry-adapted variant at finite deformations is yet to be developed. Specifically, we compute the radial polarization at multiple curvatures in the vicinity of the curvature at which the flexoelectric coefficient is desired and determine the slope from a curve fit to the data. In particular, as illustrated in Fig. 1, edge-related effects are removed by mapping the bent structure periodically in the angular direction, and the cyclic symmetry of the resultant structure is then exploited to perform highly efficient Kohn-Sham calculations [29,30,70] for the structural and electronic ground state using the Cyclix DFT code [29] — large-scale parallel implementation of cyclic+helical symmetry in state-of-the-art real-space DFT code SPARC [71,72].

We use the aforedescribed framework to calculate transversal flexoelectric coefficients for fifty-four select atomic monolayers along their principal directions. Specifically, we consider bending curvatures in the range of $0.14 < \kappa < 0.24$ nm^{-1} — resulting system sizes are intractable to traditional DFT implementations — commensurate with those found in experiments [65–68]. We select representative honeycomb lattice materials from each of Group III monochalcogenides, TMDs, Groups IV, III-V, V
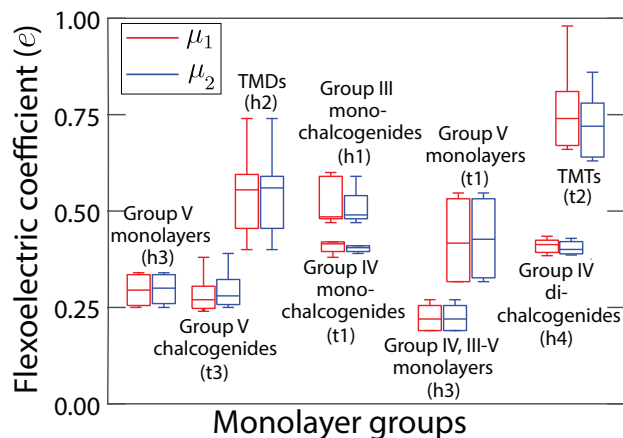
Fig. 2 Transversal flexoelectric coefficients for the select atomic monolayer groups.

monolayers, and Group IV dichalcogenides, as well as rectangular lattice materials from each of Group V monolayers, Group IV monochalcogenides, TMTs, and Group V chalcogenides. The choice of these groups is motivated by the significant success in the synthesis of affiliated monolayers, which are found to demonstrate interesting and novel properties[34–38,73–75]. Though close to half of the monolayers chosen here have not yet been synthesized, their stability has been predicted using DFT calculations[41,76], with many synthesized in multilayer form[77–81]. Therefore, we expect most, if not all, of the monolayers to be synthesized in the near future, motivating their study.

In all simulations, we employ the Perdew-Burke-Ernzerhof (PBE)[82] variant of the generalized gradient approximation (GGA) for the exchange-correlation functional and optimized norm-conserving Vanderbilt (ONCV) pseudopotentials[83] from the SG15 collection[84]. All numerical parameters, including grid spacing, k-point sampling for Brillouin zone integration, vacuum in radial direction, and structural (cell and atom) relaxation tolerances are chosen such that the computed flexoelectric coefficients are accurate to within $0.005\,e$, as verified through convergence studies (Supplementary Information). This translates to the requirement of the ground state energy being converged to within 10^{-5} Ha/atom. Note that the coefficients predicted here are expected to be reasonably robust against the two main approximations within DFT, i.e., pseudopotential and exchange-correlation functional, as dicussed next.

The equilibrium geometries for the flat monolayers computed using ABINIT[85] (Supplementary Information) are in good agreement with previous theoretical predictions[40,41] and experimental measurements[34–38,73,74]. Furthermore, the normalized difference in electron density between the PBE GGA and HSE hybrid functional[86] for the undeformed

configurations is $\mathcal{O}(1-2)$, comparable to the agreement between hybrid functionals and the gold standard Coupled Cluster Singles and Doubles (CCSD) method[87]. Similar differences are observed when spin orbit coupling is included. Since the flexoelectric coefficient is dependent on electron density differences from the flat configuration, which corresponds to small (linear) perturbations in the current context, significant error cancellations are expected. This is evidenced by recent work where both local and semilocal functionals predict nearly identical coefficients for group IV monolayers[28].

In Table 1, we present the computed transversal flexoelectric coefficients for the chosen atomic monolayers along their principal directions, which is summarized visually in Fig. 2. The variables μ_1 and μ_2 are used to represent the flexoelectric coefficient values along the x_1 and x_2 directions, respectively, whose orientation relative to the different lattice structures can be seen in Fig. 3. For honeycomb lattices, these correspond to the zigzag and armchair directions, respectively. A single value is listed in all cases since the flexoelectric coefficients are essentially constant for the bending curvatures considered here (Supplementary Information), signaling linear response for the monolayers in this regime. Note that depending on the application of interest, the flexoelectric coefficient that relates polarization to bending moment might be more informative. Therefore, the values for the so defined flexoelectric coefficient have been provided in the Supplementary Information, for which we use the bending moduli from previous work for forty-four of the materials[24], with the remaining calculated here (Supplementary Information).

The flexoelectric coefficients span a wide range of values from $0.19-0.98\,e$, with silicene and ZrTe$_3$ being at the bottom and top ends of the spectrum, respectively, and graphene towards the lower end with $0.22\,e$. In terms of the classification, Groups IV, III-V monolayers and TMTs have the smallest and largest coefficients, respectively. Interestingly, we find that the flexoelectric coefficients are similar along both principal directions, irrespective of the lattice structure. Though this is to be expected for honeycomb lattices, which usually demonstrate isotropic behavior/properties[24,76,88,89], it is most unusual for rectangular lattices, where the behavior/properties tend to be highly anistropic[24,90–93]. This is not a consequence of relaxation-related effects — cause for the bending moduli of some rectangular lattices to be isotropic[24] — which are minor in the current context (Supplementary Information). Note that when the flexoelectric coefficient relating the polarization to the bending moment is considered (Supplementary Information), the values span more than two orders of magnitude, with the trends essentially reversed,

Table 1 Transversal flexoelectric coefficient along principal directions for the fifty-four select atomic monolayers from first principles.
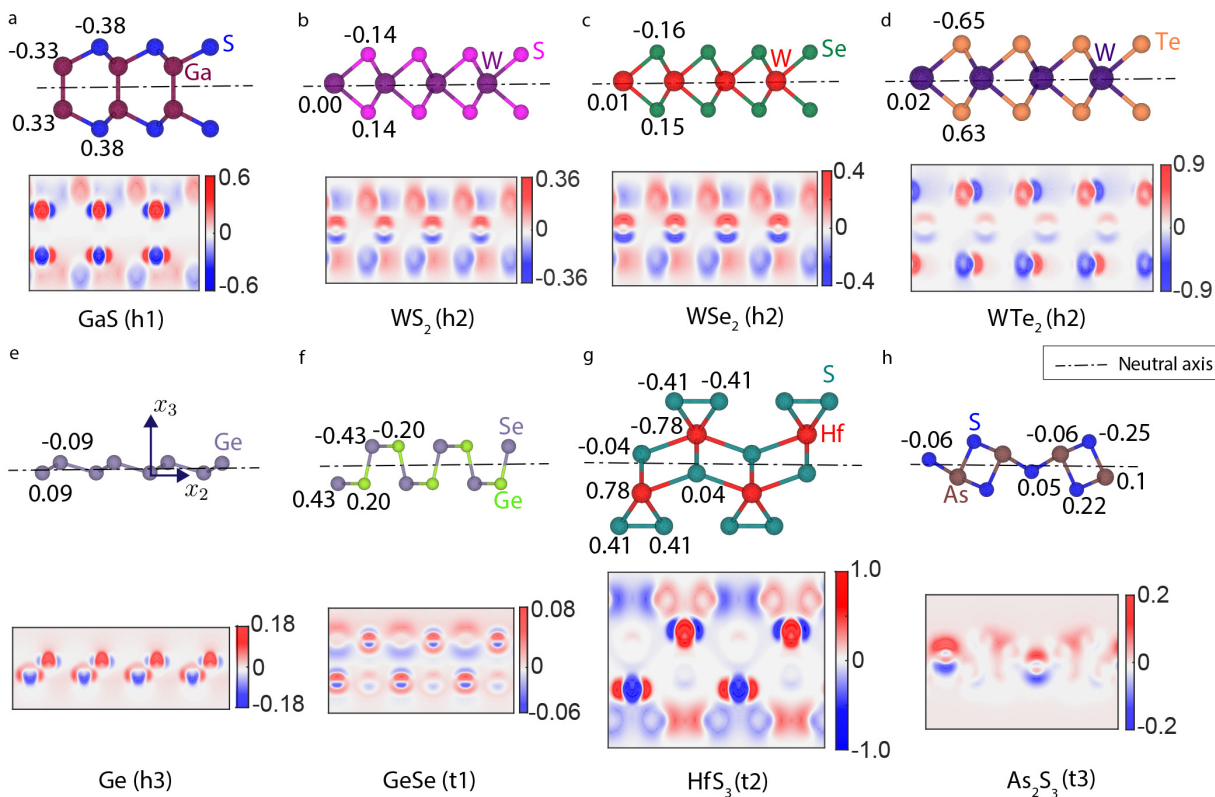
Group	Material	Flexoelectric coefficient (e)		Group	Material	Flexoelectric coefficient (e)	
		μ_1	μ_2			μ_1	μ_2
Group III monochalcogenides (h1)	GaS	0.48	0.48	Group V monolayers (h3)	P	0.25	0.25
	GaSe	0.48	0.50		As	0.26	0.27
	InS	0.47	0.47		Bi	0.33	0.33
	InSe	0.26	0.25		Sb	0.34	0.34
	InTe	0.59	0.54	Group IV dichalcogenides (h4)	$GeSe_2$	0.42	0.42
	GaTe	0.60	0.59		GeS_2	0.44	0.44
Transition metal dichalcogenides (h2)	ZrS_2	0.45	0.45		$SnSe_2$	0.40	0.41
	TiS_2	0.45	0.45		SnS_2	0.40	0.40
	$ZrSe_2$	0.46	0.47	Group V monolayers (t1)	P	0.31	0.33
	$TiSe_2$	0.41	0.40		As	0.31	0.31
	NbS_2	0.51	0.52		Bi	0.51	0.51
	$NbSe_2$	0.51	0.54		Sb	0.54	0.54
	HfS_2	0.57	0.56	Group IV monochalcogenides (t1)	GeSe	0.38	0.39
	$ZrTe_2$	0.55	0.54		GeS	0.42	0.41
	$TiTe_2$	0.58	0.56		SnSe	0.41	0.41
	$MoSe_2$	0.57	0.57		SnS	0.42	0.40
	MoS_2	0.57	0.58	Transition metal trichalcogenides (t2)	ZrS_3	0.66	0.64
	WS_2	0.59	0.59		TiS_3	0.67	0.63
	WSe_2	0.59	0.58		$ZrSe_3$	0.68	0.66
	$NbTe_2$	0.64	0.67		HfS_3	0.80	0.78
	$MoTe_2$	0.71	0.72		$HfSe_3$	0.81	0.78
	WTe_2	0.73	0.74		$ZrTe_3$	0.98	0.86
Group IV, III-V monolayers (h3)	Si	0.19	0.19	Group V chalcogenides (t3)	P_2S_3	0.24	0.25
	BN	0.20	0.20		P_2Se_3	0.25	0.26
	C	0.22	0.22		As_2S_3	0.27	0.28
	Sn	0.26	0.25		As_2Se_3	0.28	0.30
	Ge	0.27	0.27		As_2Te_3	0.38	0.39

i.e., Groups IV, III-V monolayers and TMTs now have the largest and smallest coefficients, respectively. In particular, stanene has the largest value, given its extremely small bending moduli[24], and $ZrTe_3$ has the smallest value, given its extremely large bending moduli[24]. Also, the coefficients for the rectangular lattices differ significantly in the principal directions, given their significant anisotropy in bending moduli[24].

In comparisons with experiments, while there is relatively good agreement for MoS_2 (difference of $\sim 0.09\,e$[46]), there is some disagreement for $MoSe_2$, WS_2, and WSe_2 (differences of up to $\sim 0.48\,e$[47]). These differences can be attributed to the use of a substrate, and the substantial error bars ($\sim 0.18\,e$) associated with the measurements. In comparisons to DFT-based results, the values for graphene predicted previously[50,51,53] are more than a factor of two smaller than those here. This can be attributed to the use of an ill defined flexoelectric coefficient[51] and an artificial partitioning of the electron density[50,53], as discussed in previous work[28]. The values reported previously for TMDs[52] (MX_2: M=Mo,W; X=S,Se,Te) are up two orders of magnitude smaller than those here, a consequence of using an ill defined flexoelectric coefficient and a wrinkled sheet geometry that has non-uniform strain gradients. Similarly small values for a few monolayers have been predicted very recently[62], which can be attributed to the difference in the definition of the flexoelectric coefficient. In particular, the above referenced work defines the coefficient for two-dimensional systems in terms of the drop in potential across its surfaces[62]. However, the significantly better agreement of the current results with experiments suggests the suitability of the definition adopted here[28]. Also, the current definition enables the study of large curvatures and the corresponding nonlinear response[28,95].

To get further insight into the results, considering representative materials from each group, we plot in Fig. 3 contours of electron density difference between the flat and bent monolayers for bending along the x_2 direction. We also present the charge transfer due to bending as determined via Bader analysis[94]. Similar results for bending along the x_1 direction can be found in the Supplementary Information. Three key observations can be made from

a −0.38 −0.33 S Ga 0.33 0.38 0.6 0 −0.6 GaS (h1)

b −0.14 W S 0.00 0.14 0.36 0 −0.36 WS$_2$ (h2)

c −0.16 W Se 0.01 0.15 0.4 0 −0.4 WSe$_2$ (h2)

d −0.65 W Te 0.02 0.63 0.9 0 −0.9 WTe$_2$ (h2)

e x_3 Ge −0.09 0.09 x_2 0.18 0 −0.18 Ge (h3)

f −0.43 −0.20 Se Ge 0.43 0.20 0.08 0 −0.06 GeSe (t1)

g −0.41 −0.41 S −0.78 Hf −0.04 0.78 0.04 0.41 0.41 1.0 0 −1.0 HfS$_3$ (t2)

h −0.06 S −0.06 −0.25 As 0.05 0.1 0.22 0.2 0 −0.2 As$_2$S$_3$ (t3)

−·−·− Neutral axis

Fig. 3 Contours of electron density difference (integrated along the x_1 direction) between the flat and bent ($\kappa \sim 0.2$ nm^{-1}) atomic monolayers. The contours are plotted on the x_2x_3-plane in the undeformed configuration. The charge transfer due to bending, which is shown near the corresponding atoms in the lattice structure, is obtained from Bader analysis[94].

these figures. First, charge transfer occurs from the compressive side to tensile side of the neutral axis, indicating that the origin of the flexoelectric effect for monolayers is electronic rather than ionic. The rehybridization of orbitals is likely the underlying mechanism for this effect, as previously suggested for graphene[28,50,53] and TMDs[64]. The charge transfer is similar for both bending directions, resulting in similar flexoelectric coefficients. Second, the electron density perturbations are localized near the nuclei, resulting in atomic dipoles that accumulate to generate the total radial dipole moment. The strength of these dipoles is dependent on the atom's polarizability, as evidenced from the significantly larger charge transfer for Te compared to S and Se in the tungsten dichalcogenides. Indeed, polarizability of S and Se are similar, both of which are significantly smaller than Te[96]. Third, the atomic polarization (i.e., atomic dipole per unit area) increases with distance from neutral axis, as evidenced for the S atom in the various monolayers. This can be attributed to the increase in stress with neutral axis distance.

The above observations suggest the flexoelectric coefficients for the monolayers is primarily determined by their thickness, elastic modulus along bending direction, and sum of polarizabilities of constituent atoms. The dependence on atom polarizabilities is in agreement with literature[97,98], where it has been proposed that the flexoelectric coefficient is proportional to the dielectric permittivity, which can be related to the atom polarizabilities through the Clausius–Mossotti relation[99]. Using the three features listed above, we perform a linear regression for the flexoelectric coefficients, the results of which are presented in Fig. 4. Note that the thickness has been defined to be the distance between the two atoms furthest from the neutral axis plus an additional 11 Bohr (results insensitive to this choice ±4 Bohr). This choice is based on the typical out-of-plane extent of atomic orbitals/electron density. Indeed, the structural thickness so defined can differ from the effective thickness of the monolayer[69]. The regression fit is very good, suggesting that the flexoelectric coefficients for atomic monolayers are primarily decided by the three aforementioned features. Though the quality of fit can be further increased by using higher order polynomial regression (Supplementary Information), it can possibly lead to overfitting, and hence not chosen here.

In Fig. 4, we perform a linear regression between the flexoelectric coefficients and each of the aforementioned features independently. The fits are not as good as with the three-feature regression, suggesting that any one indi-
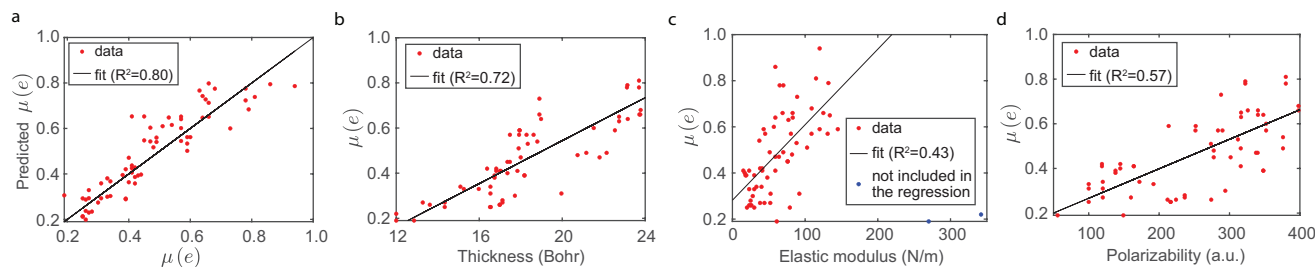
Fig. 4 (a) Set of calculated transversal flexoelectric coefficients and its linear regression with the features being thickness, elastic modulus along bending direction, and sum of polarizability of constituent atoms. (b), (c), and (d) Set of computed flexoelectric coefficients and its linear regression with each of the features independently. In all plots, R^2 denotes the coefficient of determination for the regression.

vidual feature is insufficient to make accurate predictions. This is because of the inherent dependence of the flexoelectric coefficients on all three features, further verifying that they are all instrumental in determining the strength of the flexoelectric effect. Indeed, the correlation coefficient with each individual feature is proportional to the corresponding coefficient in the three-feature linear regression, indicating that monolayer thickness has the maximum impact on the flexoelectric coefficient. Overall, though there are a number of exceptions, the results suggest that the flexoelectric coefficient generally increases with monolayer thickness, elastic modulus along bending direction, and sum of polarizability of constituent atoms. Indeed, given the complex nature of the bonding in atomic monolayers, ab initio DFT calculations such as those employed in the current work are required for accurate predictions.

In summary, we have studied the flexoelectric effect in atomic monolayers using first principles DFT. Specifically, considering representative materials from each of the prominent monolayer groups, we have computed the transversal flexoelectric coefficients for fifty-four select monolayers along their principal directions at practically relevant bending curvatures using symmetry-adapted DFT calculations. We have found that the monolayers demonstrate linear behavior and have similar flexoelectric coefficients along both principal directions, with values for TMTs being up to a factor of five larger than graphene. In addition, we have found electronic origins for the flexoelectric effect, which increases with monolayer thickness, elastic modulus along bending direction, and sum of polarizability of constituent atoms.

Overall, this work provides an important reference for the transversal flexoelectric coefficients for a number of important atomic monolayers, and provides fundamental insights into the underlying mechanisms. The flexoelectric coefficients predicted here could prove useful in the design of nanoelectromechanical devices, with the regression model in terms of the three aforementioned features

serving as a powerful tool for rapid preliminary searches through large databases of two-dimensional materials. Indeed, the symmetry-adapted DFT calculations employed here, which can calculate the coefficient for a material in a few minutes on a few hundred processors, are likely to serve as a useful tool for searches through small to moderate-sized databases. The study of the flexoelectric effect in bilayer and multilayer materials, where tremendously large coefficients have been predicted[100], is a worthy subject for future research.
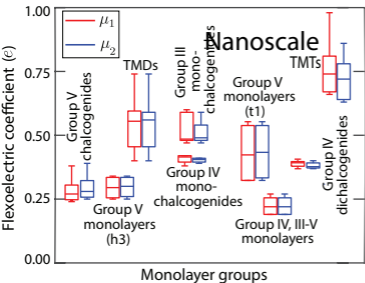
Acknowledgments

Conflicts of interest

There are no conflicts to declare.

References

1   A. K. Tagantsev, *Phase Transit.*, 1991, **35**, 119–203.
2   P. Yudin and A. Tagantsev, *Nanotechnology*, 2013, **24**, 432001.
3   P. Zubko, G. Catalan and A. K. Tagantsev, *Annual Review of Materials Research*, 2013, **43**, 387–421.
4   T. D. Nguyen, S. Mao, Y.-W. Yeh, P. K. Purohit and M. C. McAlpine, *Advanced Materials*, 2013, **25**, 946–974.
5   F. Ahmadpoor and P. Sharma, *Nanoscale*, 2015, **7**, 16555–16570.
6   J. Narvaez, F. Vasquez-Sancho and G. Catalan, *Nature*, 2016, **538**, 219–221.
7   S. Krichen and P. Sharma, *Journal of Applied Mechanics*, 2016, **83**,.
8   B. Wang, Y. Gu, S. Zhang and L.-Q. Chen, *Prog. Mater. Sci.*, 2019, **106**, 100570.
9   E. W. Hill, A. Vijayaragahvan and K. Novoselov, *IEEE Sensors Journal*, 2011, **11**, 3161–3170.
10 Q.-M. Wang, X.-H. Du, B. Xu and L. E. Cross, *IEEE transactions on ultrasonics, ferroelectrics, and frequency control*, 1999, **46**, 638–646.
11 S. Xu, Y. Qin, C. Xu, Y. Wei, R. Yang and Z. L. Wang, *Nature nanotechnology*, 2010, **5**, 366–373.
12 X. Wang, H. Tian, W. Xie, Y. Shu, W.-T. Mi, M. A. Mohammad, Q.-Y. Xie, Y. Yang, J.-B. Xu and T.-L. Ren, *NPG Asia Materials*, 2015, **7**, e154–e154.
13 G. da Cunha Rodrigues, P. Zelenovskiy, K. Romanyuk, S. Luchkin, Y. Kopelevich and A. Kholkin, *Nature communications*, 2015, **6**, 1–6.

14 J. Pu, Y. Yomogida, K.-K. Liu, L.-J. Li, Y. Iwasa and T. Takenobu, *Nano Letters*, 2012, **12**, 4013–4017.

15 G.-H. Lee, Y.-J. Yu, X. Cui, N. Petrone, C.-H. Lee, M. S. Choi, D.-Y. Lee, C. Lee, W. J. Yoo, K. Watanabe, T. Taniguchi, C. Nuckolls, P. Kim and J. Hone, *ACS Nano*, 2013, **7**, 7931–7936.

16 G. A. Salvatore, N. Munzenrieder, C. Barraud, L. Petti, C. Zysset, L. Buthe, K. Ensslin and G. Troster, *ACS Nano*, 2013, **7**, 8809–8815.

17 J. Yoon, W. Park, G.-Y. Bae, Y. Kim, H. SooJang, Y. Hyun, S. K. Lim, Y. H. Kahng, W.-K. Hong, B. H. Lee and H. C. Ko, *Small*, 2013, **9**, 3295–3300.

18 Y. Zhang, B. Zheng, C. Zhu, X. Zhang, C. Tan, H. Li, B. Chen, J. Yang, J. Chen, Y. Huang, L. Wang and H. Zhang, *Advanced Materials*, 2015, **27**, 935–939.

19 A. Sakhaee-Pour, M. Ahmadian and A. Vafai, *Solid State Communications*, 2008, **147**, 336–340.

20 V. Sazonova, Y. Yaish, H. Üstünel, D. Roundy, T. A. Arias and P. L. McEuen, *Nature*, 2004, **431**, 284.

21 J. S. Bunch, A. M. V. D. Zande, S. S. Verbridge, I. W. Frank, D. M. Tanenbaum, J. M. Parpia, H. G. Craighead and P. L. McEuen, *Science*, 2007, **315**, 490–493.

22 K. Novoselov and A. C. Neto, *Physica Scripta*, 2012, **2012**, 014006.

23 Y. Qin, Q. Peng, Y. Ding, Z. Lin, C. Wang, Y. Li, F. Xu, J. Li, Y. Yuan, X. He and Y. Li, *ACS Nano*, 2015, **9**, 8933–8941.

24 S. Kumar and P. Suryanarayana, *Nanotechnology*, 2020, **31**, 43LT01.

25 U. K. Bhaskar, N. Banerjee, A. Abdollahi, E. Solanas, G. Rijnders and G. Catalan, *Nanoscale*, 2016, **8**, 1293–1298.

26 A. Abdollahi and I. Arias, *Journal of Applied Mechanics*, 2015, **82**, 121003(1–4).

27 A. Abdollahi, N. Domingo, I. Arias and G. Catalan, *Nature Communications*, 2019, **10**, 1266.

28 D. Codony, I. Arias and P. Suryanarayana, *arXiv preprint arXiv:2010.01747*, 2020.

29 A. Sharma and P. Suryanarayana, 2020.

30 S. Ghosh, A. S. Banerjee and P. Suryanarayana, *Physical Review B*, 2019, **100**, 125143.

31 R. Mas-Balleste, C. Gomez-Navarro, J. Gomez-Herrero and F. Zamora, *Nanoscale*, 2011, **3**, 20–30.

32 S. Z. Butler, S. M. Hollen, L. Cao, Y. Cui, J. A. Gupta, H. R. Gutiérrez, T. F. Heinz, S. S. Hong, J. Huang, A. F. Ismach, E. Johnston-Halperin, M. Kuno, V. V. Plashnitsa, R. D. Robinson, R. S. Ruoff, S. Salahuddin, J. Shan, L. Shi, M. G. Spencer, M. Terrones, W. Windl and J. E. Goldberger, *ACS Nano*, 2013, **7**, 2898–2926.

33 D. Geng and H. Y. Yang, *Advanced Materials*, 2018, **30**, 1800865.

34 S. Balendhran, S. Walia, H. Nili, S. Sriram and M. Bhaskaran, *Small*, 2015, **11**, 640–652.

35 S. Zhou, C.-C. Liu, J. Zhao and Y. Yao, *npj Quantum Materials*, 2018, **3**, 1–7.

36 D. D. Vaughn, R. J. Patel, M. A. Hickner and R. E. Schaak, *Journal of the American Chemical Society*, 2010, **132**, 15170–15172.

37 S. Zhang, S. Guo, Z. Chen, Y. Wang, H. Gao, J. Gómez-Herrero, P. Ares, F. Zamora, Z. Zhu and H. Zeng, *Chemical Society Reviews*, 2018, **47**, 982–1021.

38 J. Dai, M. Li and X. C. Zeng, *Wiley Interdisciplinary Reviews: Computational Molecular Science*, 2016, **6**, 211–222.

39 C. Wang, C. Zheng and G. Gao, *The Journal of Physical Chemistry C*, 2020, **124**, 6536–6543.

40 S. Haastrup, M. Strange, M. Pandey, T. Deilmann, P. S. Schmidt, N. F. Hinsche, M. N. Gjerding, D. Torelli, P. M. Larsen, A. C. Riis-Jensen, J. Gath, K. W. Jacobsen, J. J. Mortensen, T. Olsen and K. S. Thygesen, *2D Materials*, 2018, **5**, 042002.

41 J. Zhou, L. Shen, M. D. Costa, K. A. Persson, S. P. Ong, P. Huck, Y. Lu, X. Ma, Y. Chen, H. Tang and Y. P. Feng, *Scientific data*, 2019, **6**, 1–10.

42 N. Kerszberg and P. Suryanarayana, *RSC Advances*, 2015, **5**, 43810–43814.

43 R. Fei, W. Li, J. Li and L. Yang, *Applied Physics Letters*, 2015, **107**, 173104.

44 Y.-T. Hsu, A. Vaezi, M. H. Fischer and E.-A. Kim, *Nature communications*, 2017, **8**, 1–6.

45 X.-F. Jiang, Q. Weng, X.-B. Wang, X. Li, J. Zhang, D. Golberg and Y. Bando, *Journal of Materials Science & Technology*, 2015, **31**, 589–598.

46 C. J. Brennan, R. Ghosh, K. Koul, S. K. Banerjee, N. Lu and E. T. Yu, *Nano Letters*, 2017, **17**, 5464–5471.

47 C. J. Brennan, K. Koul, N. Lu and E. T. Yu, *Applied Physics Letters*, 2020, **116**, 053101.

48 P. Hohenberg and W. Kohn, *Physical Review*, 1964, **136**, B864–B871.

49 W. Kohn and L. J. Sham, *Physical Review*, 1965, **140**, A1133–A1138.

50 T. Dumitrică, C. M. Landis and B. I. Yakobson, *Chemical physics letters*, 2002, **360**, 182–188.

51 S. V. Kalinin and V. Meunier, *Physical Review B*, 2008, **77**, 033403.

52 W. Shi, Y. Guo, Z. Zhang and W. Guo, *The journal of physical chemistry letters*, 2018, **9**, 6841–6846.

53 A. G. Kvashnin, P. B. Sorokin and B. I. Yakobson, *The journal of physical chemistry letters*, 2015, **6**, 2740–2744.

54 X. Gonze and C. Lee, *Phys. Rev. B*, 1997, **55**, 10355.

55 S. Baroni, S. De Gironcoli, A. Dal Corso and P. Giannozzi, *Rev. Mod. Phys.*, 2001, **73**, 515.

56 J. Hong and D. Vanderbilt, *Physical Review B*, 2011, **84**, 180101.

57 J. Hong and D. Vanderbilt, *Phys. Rev. B*, 2013, **88**, 174107.

58 M. Stengel, *Phys. Rev. B*, 2013, **88**, 174106.

59 M. Stengel, *Phys. Rev. B*, 2014, **90**, 201112(R).

60 C. E. Dreyer, M. Stengel and D. Vanderbilt, *Phys. Rev. B*, 2018, **98**, 075153.

61 M. Royo and M. Stengel, *Physical Review X*, 2019, **9**, 021050.

62 M. Springolo, M. Royo and M. Stengel, *arXiv preprint arXiv:2010.08470*, 2020.

63 B. Javvaji, B. He, X. Zhuang and H. S. Park, *Physical Review Materials*, 2019, **3**, 125402.

64 X. Zhuang, B. He, B. Javvaji and H. S. Park, *Physical Review B*, 2019, **99**, 054105.

65 N. Lindahl, D. Midtvedt, J. Svensson, O. A. Nerushev, N. Lindvall, A. Isacsson and E. E. Campbell, *Nano Letters*, 2012, **12**, 3526–3531.

66 E. Han, J. Yu, E. Annevelink, J. Son, D. A. Kang, K. Watanabe, T. Taniguchi, E. Ertekin, P. Y. Huang and A. M. van der Zande, *Nature materials*, 2019, 1–5.

67 G. Wang, Z. Dai, J. Xiao, S. Feng, C. Weng, L. Liu, Z. Xu, R. Huang and Z. Zhang, *Physical Review Letters*, 2019, **123**, 116101.

68 W. Qu, S. Bagchi, X. Chen, H. B. Chew and C. Ke, *Journal of Physics D: Applied Physics*, 2019, **52**, 465301.

69 Y. Huang, J. Wu and K.-C. Hwang, *Physical review B*, 2006, **74**, 245413.

70 A. S. Banerjee and P. Suryanarayana, *Journal of the Mechanics and Physics of Solids*, 2016, **96**, 605–631.

71 Q. Xu, A. Sharma, B. Comer, H. Huang, E. Chow, A. J. Medford, J. E. Pask and P. Suryanarayana, *arXiv preprint arXiv:2005.10431*, 2020.

72 S. Ghosh and P. Suryanarayana, *Computer Physics Communications*, 2017, **216**, 109–125.

73 J. N. Coleman, M. Lotya, A. O'Neill, S. D. Bergin, P. J. King, U. Khan, K. Young, A. Gaucher, S. De, R. J. Smith, I. V. Shvets, S. K. Arora, G. Stanton, H.-Y. Kim, K. Lee, G. T. Kim, G. S. Duesberg, T. Hallam, J. J. Boland, J. J. Wang, J. F. Donegan, J. C. Grunlan, G. Moriarty, A. Shmeliov, R. J. Nicholls, J. M. Perkins, E. M. Grieveson, K. Theuwissen, D. W. McComb, P. D. Nellist and V. Nicolosi, *Science*, 2011, **331**, 568–571.

74 K. S. Novoselov, D. Jiang, F. Schedin, T. J. Booth, V. V. Khotkevich, S. V. Morozov and A. K. Geim, *Proceedings of the National Academy of Sciences*, 2005, **102**, 10451–10453.

75 M. Šiškins, M. Lee, F. Alijani, M. R. van Blankenstein, D. Davidovikj, H. S. van der Zant and P. G. Steeneken, *ACS nano*, 2019, **13**, 10845–10851.

76 F. A. Rasmussen and K. S. Thygesen, *The Journal of Physical Chemistry C*, 2015, **119**, 13169–13183.

77 R. Dong, T. Zhang and X. Feng, *Chemical reviews*, 2018, **118**, 6189–6235.

78 Z. Hu, Y. Ding, X. Hu, W. Zhou, X. Yu and S. Zhang, *Nanotechnology*, 2019, **30**, 252001.

79 P. Hu, Z. Wen, L. Wang, P. Tan and K. Xiao, *ACS nano*, 2012, **6**, 5988–5994.

80 G. W. Mudd, S. A. Svatek, T. Ren, A. Patanè, O. Makarovsky, L. Eaves, P. H. Beton, Z. D. Kovalyuk, G. V. Lashkarev, Z. R. Kudrynskyi and A. I. Dmitriev, *Advanced Materials*, 2013, **25**, 5714–5718.

81 W. Gao and J. R. Chelikowsky, *Nano Letters*, 2020, **20**, 8346–8352.

82 J. P. Perdew and W. Yue, *Physical Review B*, 1986, **33**, 8800.

83 D. R. Hamann, *Physical Review B*, 2013, **88**, 085117.

84 M. Schlipf and F. Gygi, *Computer Physics Communications*, 2015, **196**, 36 – 44.

85 X. Gonze, J. M. Beuken, R. Caracas, F. Detraux, M. Fuchs, G. M. Rignanese, L. Sindic, M. Verstraete, G. Zerah, F. Jollet, M. Torrent, A. Roy, M. Mikami, P. Ghosez, J. Y. Raty and D. C. Allan, *Computational Materials Science*, 2002, **25**, 478–492(15).

86 J. Heyd, G. E. Scuseria and M. Ernzerhof, *The Journal of chemical physics*, 2003, **118**, 8207–8215.

87 M. G. Medvedev, I. S. Bushmarinov, J. Sun, J. P. Perdew and K. A. Lyssenko, *Science*, 2017, **355**, 49–52.

88 H. Ding, Z. Zhen, H. Imtiaz, W. Guo, H. Zhu and B. Liu, *Extreme Mechanics Letters*, 2019, **32**, 100507.

89 W. Li and J. Li, *Nano Research*, 2015, **8**, 3796–3802.

90 L. Li, W. Han, L. Pi, P. Niu, J. Han, C. Wang, B. Su, H. Li, J. Xiong, Y. Bando and T. Zhai, *InfoMat*, 2019, **1**, 54–73.

91 F. Xia, H. Wang and Y. Jia, *Nature Communications*, 2014, **5**, 1–6.

92 X. Wang, A. M. Jones, K. L. Seyler, V. Tran, Y. Jia, H. Zhao, H. Wang, L. Yang, X. Xu and F. Xia, *Nature Nanotechnology*, 2015, **10**, 517–521.

93 Z. Luo, J. Maassen, Y. Deng, Y. Du, R. P. Garrelts, M. S. Lundstrom, D. Y. Peide and X. Xu, *Nature Communications*, 2015, **6**, 1–8.

94 R. Bader and T. Nguyen-Dang, in *Advances in Quantum Chemistry*, Elsevier, 1981, vol. 14, pp. 63–124.

95 D. Codony, P. Gupta, O. Marco and I. Arias, *J. Mech. Phys. Sol.*, 2020, **146**, 104182.

96 H. Tandon, T. Chakraborty and V. Suhag, *Journal of Mathematical Chemistry*, 2019, **57**, 2142–2153.

97 A. Tagantsev, *Zhurnal Eksperimental'noi i Teoreticheskoi Fiziki*, 1985, **88**, 2108–22.

98 L. L. Ma, W. J. Chen and Y. Zheng, in *Flexoelectric Effect at the Nanoscale*, ed. S. Schmauder, C.-S. Chen, K. K. Chawla, N. Chawla, W. Chen and Y. Kagawa, Springer Singapore, Singapore, 2019, pp. 549–589.

99 D. J. Griffiths, *Introduction to Electrodynamics*, Cambridge University Press, 4th edn., 2017.

100 K.-A. N. Duerloo and E. J. Reed, *Nano letters*, 2013, **13**, 1681–1686.

Flexoelectric coefficient (e)

Monolayer groups

Group V chalcogenides

TMDs

Group III mono-chalcogenides

Group IV mono-chalcogenides

Group V monolayers (h3)

Group V monolayers (t1)

Group IV, III-V monolayers

TMTs

Group IV dichalcogenides

μ_1

μ_2

Dipole moment

$1/\kappa$

O